ATOTP0104US

IN THE UNITED STATES PATENT AND TRADEMARK OFFICE

In re application of:

Nayan H. Joshi et al	:	Group Art Unit: 1762
Application No.: 10/606,460	:	Examiner: Katherine A. Bareford
Filed: 26 June 2003	:	Confirmation No. 3492

For: AQUEOUS ACIDIC IMMERSION PLATING SOLUTIONS AND METHODS FOR PLATING ON ALUMINUM AND ALUMINUM ALLOYS

DECLARATION UNDER 37 C.F.R. 1.132 OF NAYAN H. JOSHI

VIA EFS
M/S Amendment
Commissioner for Patents
P.O. Box 1450
Alexandria, VA 22313-1450

Sir:

I, Nayan H. Joshi, declare and say as follows:

(1) I am a co-inventor of U.S. Application No. 10/606,460 ("the present application"). At present, I am General Metals Finishing (GMF) R&D Manager at Atotech U.S.A., a subsidiary of the assignee of the present application. I hold a M.S. degree in inorganic chemistry, awarded by Saurashtra University (India) in 1975, and Ph.D. degree in electrochemistry-metallic corrosion, awarded by Gujarat University (India) in 1980. Following these degrees, I worked in several institutions and companies in India, until coming to the U.S. in 1984. I began working at M&T Chemicals in 1988, which subsequently became Atotech U.S.A. in 1992. I have been employed by Atotech U.S.A. since. I have previously submitted a list of my publications

and patents in the present application. Based on these facts, I consider myself, and believe my colleagues consider me, to be a person of skill in the art of metal finishing, including in particular the immersion plating art relevant to the present application.

(2) The present application includes claims drawn to an acidic immersion metal deposition process for depositing a zinc alloy protective coating on aluminum or aluminum based alloy substrates. The process forms a thin protective layer which is intended and used to protect the aluminum or aluminum alloy substrate from formation of an oxide on the surface prior to application of subsequent layers, which otherwise would occur very quickly and in such manner that an unsatisfactory deposit would be obtained, over which subsequently applied layers would not properly deposit. The process of the present invention is not intended to provide a final finish, but is intended simply to protect the surface until a subsequently applied, much thicker layer of, e.g., nickel, is deposited on the substrate by electroless plating and/or by electroplating. The process is neither intended to nor is able to deposit a thick metal deposit. The present invention provides an alternative to previously known alkaline zincate treatments. The present invention avoids the necessity of hard complexing agents including cyanide ions and makes the pre-plate treatment for aluminum friendlier to the environment, avoids the necessity of the double treatment required in alkaline zincate treatments, and avoids the use of the highly alkaline compositions of the prior art zincate processes. One of the critical factors in obtaining the desired deposit is the use of acetate as the counter ion for the source of zinc, nickel and/or cobalt that is used in forming the immersion plating bath that forms the deposit. Use of this counter ion, in combination with the inhibitor, provides an unexpectedly very excellent, very thin protective zinc alloy coating on the aluminum or aluminum alloy substrate. The process of the present invention bears little or no resemblance to any known process for applying zinc alloy coatings on an aluminum or aluminum alloy substrate.

(3) It is my understanding that the claims of the present application have been rejected as obvious over the combination of U.S. Patent No. 2,580,773, to Heiman, with U.S. Patent No. 5,405,523, to Eckles, and further in view of U.S. Patent No. 2,892,760 to Gündel or U.S. Patent No. 3,960,677 to Hildering. It is my understanding that the Examiner contends that it would have been obvious, first, to have modified the Heiman immersion bath, to use the pH range of the Eckles electroplating bath; second, thence to have further modified the Eckles pH range to the claimed range; third, to have further modified Heiman by the addition of an electroplating brightener taught by Eckles only for use in an electroplating bath; fourth, to have optimized the ranges of materials; fifth, to immediately, without having used it first, further modify the combination of Heiman and Eckles by discarding the Eckles brighter in favor of the brightener taught by either of Gündel or Hildering which, by its presence, would function as Applicants' claimed inhibitor; and sixth, to have selected acetate as counter ion. Finally after having made these sequential, stepwise series of allegedly obvious modifications, the Examiner contends that the person of ordinary skill in the art would have found Applicants' invention obvious. I have carefully reviewed all of the references cited by the Examiner in rejecting the claims of the application and the lengthy stepwise rationale for selecting from and modifying the various teachings of these references as contended.

(4) It is my further understanding that the claims of the present application have been rejected as obvious over the combination of JP 2000-256864 ("JP '864"), with U.S. Patent No. 5,182,006, to Haydu, and further in view of Gündel or Hildering. It is my understanding that the Examiner contends that it would have been obvious, first, to have modified JP '864 by applying the cleaning process of Haydu; second, thence to have added the specific alkaline zincate brightener of Haydu to the acidic immersion plating composition of JP '864; third, to immediately, without having used it first, further

modify the combination of JP '864 and Haydu by discarding the Haydu brighter in favor of the brightener taught by either of Gündel or Hildering which, by its presence, would function as Applicants' claimed inhibitor; and fourth, to have selected acetate as counter ion. Finally after having made these sequential, stepwise series of allegedly obvious modifications, the Examiner contends that the person of ordinary skill in the art would have found Applicants' invention obvious. I have carefully reviewed all of the references cited by the Examiner in rejecting the claims of the application and the lengthy stepwise rationale for selecting from and modifying the various teachings of these references as contended.

(5) As a person of skill in the art of metal surface treatment including, in particular, immersion plating processes such as those of the presently claimed invention, I cannot agree that, when taken as a whole, the presently claimed invention would have been obvious in view of the collection of prior art cited and relied upon by the Examiner, and referred to in paragraphs (3) and (4) above. This series of selections and modifications is such an unlikely and improbably series that it is simply not reasonable to contend that it would have been obvious, even for a person of skill in the art, to have followed this path and carried out this series.

This sequential series of selections and modifications of the selections is not something that would have been obvious to the skilled person in the art, much less to a person of ordinary skill in the art. While the Examiner has offered a rationale for each of the individual steps, each taken one at a time and followed by subsequent modifications, the Examiner has not stated why or how the invention as a whole would have been obvious to a person such as myself, or to a person of ordinary skill in the art. There are simply too many stepwise changes, followed by subsequent changes of the preceding changes to reasonably be considered to have been obvious. The route from the Heiman reference or from the JP '864 reference to the presently claimed invention

would not have been at all obvious to the person of ordinary skill in the art. In hindsight, the immersion plating bath used in the claimed process may appear like a simple combination. However, the work leading up to the present invention was not a simple or obvious combination, but was instead the result of a painstaking research and development effort that eventually arrived at the present invention, which is a significant improvement over the prior art zincating processes.

(6) It is my understanding that the Examiner's rejections all rely upon the premise that it would have been obvious to select any given electroplating brightener, and specifically, the brighteners disclosed by the Gundel and Hildering references, which are known for use only in quite distinct electroplating processes, and to include such brightener in a zinc-nickel immersion plating bath such as that presently claimed. With all due respect to the Examiner's experience and knowledge of the patent literature and of the metal surface treatment art, I cannot agree that any such selection would have been obvious. Throughout the prosecution of this application, the Applicants have shown facts and repeatedly argued that, (1) the selection of any given brightener is a highly empirical, trial-and-error undertaking, and (2) the fact that a given additive, e.g., a brightener, works in an electroplating bath would not be considered sufficient to raise any reasonable expectation that the same additive would work in a chemical plating bath, such as an immersion plating bath as a brightener or for any particular purpose. In addition to the previously-submitted evidence in support of this point, included with this Declaration is a copy of McFadden, G.B., et al., "A Mechanism for Brightening: Linear Stability Analysis of the Curvature-Enhanced Coverage Model", J. of the Electrochemical Society, 150 (9) C591-C599 (2003) ("McFadden et al."). As stated by McFadden et al. on page C591:

> For this reason, electrolytes commonly used for industrial plating applications that require optically bright deposits typically contain a

> variety of additives that have been empricially determined to yield bright deposits. *There is no fundamental basis for determining which additives to add or why.* (Emphasis added.)

As clearly stated by McFadden et al., plating additives are selected on an empirical basis, and most importantly, *there is no fundamental basis for determining which additives to add or why.* McFadden et al. is attached hereto as Exhibit A.

That is, there is no way to predict which additive is going to work in any given plating system. The mere fact that any given compound is known for use as a brightener in a given electroplating process is not evidence to create an expectation or a rational basis for selecting that given compound for use in a completely different plating bath having completely different chemistry and, in particular, having a completely different mode of deposition of metal onto substrate. For this reason alone, as a person of skill in the art, I cannot accept the Examiner's position that it would have been obvious to employ the electroplating brighteners disclosed by Gundel or Hildering in an immersion plating bath such as that presently disclosed and claimed.

Finally, it is noteworthy that the McFadden et al. paper is contemporaneous with the present application, and thus clearly shows that, at the time the presently claimed invention was made, there would have been no logical or rational basis for selecting any given brightener for use in any electroplating process, much less in an immersion plating process, in which such an inherently very thin coating could hardly benefit from a brightener.

(7) To the extent that the Examiner relies upon the teachings in Haydu et al. of a brighter in a zincating process, as would be readily understood by those of skill in the art, zincating is carried out at high pH and the chemical mechanism by which the zinc coating is deposited is quite different from the immersion plating at slightly acidic pH of the present invention. Such zincating processes generally deposit a thicker

coating than does the immersion plating process of the present invention. Such a thicker coating could possibly benefit from a brightener, to the extent that it actually is a "brightener" and not simply a deposition aid. The fact that a zincating process such as that of Haydu et al. may benefit from the addition of a compound known for use as a brightener in other electroplating processes does not in any way lead to the conclusion or even suggestion that addition of a brightener to an immersion plating process such as that of the present invention would have any benefit at all. Any such suggestion is nothing more than speculation.

(8) In making the present invention, and in order to support my statements in the foregoing paragraphs, Applicants, including myself and others working under my direction, have conducted a series of experiments, reported in the following paragraphs. It is important to understand that the purpose of the present invention is not to provide a final coating on the aluminum or aluminum alloy; it is not to provide a "bright" coating; and, it is not to provide a thick or heavy coating. The purpose is, instead, to provide a very thin, protective coating on the aluminum or aluminum alloy, a coating that will prevent the formation of the native oxide layer which would otherwise occur very quickly after the aluminum surface is desmutted and cleaned. In order to obtain such a coating, it was discovered by the present inventors that it is necessary to slow down the reaction, due to the high immersion plating reactivity of aluminum. This has been accomplished by making three major modifications. The first modification is to use the acetate form of the zinc and nickel (and/or cobalt, when used) sources. As shown below, due to its lower reactivity with aluminum, the acetate works much better than would the normally-used, less expensive and more easily commercially available but more aluminum-reactive chloride or sulfate salts. The second modification is to use the inhibitor to further slow the rate of reaction. The third modification is to use a mildly acidic pH range, i.e., 4.5-5.5, to even further slow the rate of reaction. The following

paragraphs set forth the experimental results demonstrating the unexpected benefits of the claimed combination of bath components in the immersion plating bath used in the presently claimed process.

(9) Many of the tests conducted both in the course of development of the present invention and in the prosecution of the present patent application have been directed to two very different alloys of aluminum, the 6061 alloy and the 2024 alloy. As is known in the art, these two alloys contain a significantly different combination of alloying elements. As a result, for the purposes of the present invention, these two alloys represent relative extremes of the range of reactivity with the composition used in the claimed immersion plating process. "Pure", non-alloyed aluminum would fall somewhere between these two extremes. Commercially, it is considered that, if a given immersion plating process works satisfactorily on both of these alloys, it will most likely work satisfactorily on any aluminum or aluminum alloy. Thus, the 6061 alloy and the 2024 alloy are considered both by me and in the art generally to be representative of aluminum and aluminum alloys generally. The industry-accepted compositions of these two alloys are shown in the following table:

6061	2024
Aluminum Balance	Aluminum Balance
Chromium 0.04 - 0.35	Chromium 0.1 max
Copper 0.15 - 0.4	Copper 3.8 - 4.9
Iron 0 - 0.7	Iron 0.5 max
Magnesium 0.8 - 1.2	Magnesium 1.2 - 1.8
Manganese 0.15 max	Manganese 0.3 - 0.9
Other 0.15 max	Remainder Each 0.05 max
Remainder Each 0.05 max	Remainder Total 0.15 max
Silicon 0.4 - 0.8	Silicon 0.5 max
Titanium 0.15 max	
Zinc 0.25 max	Zinc 0.25 max

For example, in the 2024 alloy the high copper content has a significant negative effect

on the reactivity of the alloy in zinc-nickel immersion plating. If too much of or too strong an inhibitor is added to the immersion plating bath, no deposition of immersion metal will take place. The 6061 alloy, on the other hand, is relatively highly reactive and to obtain a desirably good deposition of immersion metal while avoiding a "runaway" reaction, a significant amount of the inhibitor is needed. While it might be possible for a given plating operation to adjust the conditions for each alloy, what is commercially necessary and desirable is a single immersion plating bath that can apply a desirably good deposition of immersion metal to the full range of aluminum and aluminum alloys that are used commercially. It is not desirable to have, and customers would not accept, a plurality of different immersion plating baths, each one directed to a specific aluminum alloy. For these reasons, the use of the two aluminum alloys, i.e., the 6061 alloy and the 2024 alloy, are considered representative of the aluminum and aluminum alloys in general.

(10) During the development of the presently claimed invention, it was discovered that the acetates of zinc and nickel provided a much improved immersion deposit as compared to the chlorides or sulfates. This is demonstrated and exemplified in the following results:

Bath Component	Formulation I	Formulation II	Formulation III	Formulation IV
$SnCl_2$, anhyd.	150 g/l	-	-	-
$ZnCl_2$, anhyd.	50 g/l	200 g/l	-	-
HCl (37%)	100 ml/l	100 ml/l	100 ml/l	-
$[NH_4][HF_2]$	50 g/l	50 gm/l	50 gm/l	3 g/l
Acetic acid (glacial)	50 ml/l	50 g/l	50 ml/l	-
$MnSO_4 \cdot H_2O$	-	10 g/l	10 g/l	-
$NiCl_2 \cdot 6H_2O$	-	-	250 g/l	-
$CuSO_4 \cdot 5H_2O$	-	-	1 g/l	-
Ni acetate$\cdot 4H_2O$	-	-	-	70 g/l
Zn acetate$\cdot 2H_2O$	-	-	-	30 g/l
Water	Balance	Balance	Balance	Balance
RESULTS:				
Action on Alloy	very aggressive	moderate	aggressive	very mild
Adhesion 2024	loose, powdery	loose, powdery	loose, powdery	good
Adhesion 6061	loose, powdery	loose, powdery	fair	fair, satisfactory

Each of the foregoing immersion plating baths was prepared as shown above, and the specified aluminum alloy (alloys 2024 and 6061) strips were immersed in the respective baths for two minutes at room temperature. The treated panels were then plated in an

electroless nickel plating bath for a time sufficient to deposit about 25 microns of nickel metal on the immersion-deposited zinc-nickel alloy. The nickel-plated panels were then checked for adhesion using the 90° bend test. As shown by the above results, only the acetate-based zinc/nickel bath obtained a deposit having fair or good adhesion to both alloys and having only very mild action on the alloy surface. It is noted that these tests were conducted in the absence of the claimed inhibitors, which are provided for the purpose of improving the quality of the deposit by further reducing any deleterious effect on the aluminum or aluminum alloy surface resulting from the immersion plating bath chemistry.

(11) In preparation of the present Declaration, Applicants have conducted comparative testing to show that the acetate counter ion provides much superior results compared to either the chloride or the sulfate counter ion for the zinc and nickel ions in the immersion plating baths used in the process of the present invention. It is noted that nitrate baths were not tested, because the nitrate salts of nickel and zinc are highly oxidizing, especially to aluminum, and in fact form the very oxide layer sought to be avoided by the present invention. Due to its oxidizing activity, nitrate salts are not used for plating applications and were not used in these experiments.

Applicants prepared the solutions shown in the table shown below. The bath in example 11 corresponds to Example C in Table I of the present specification at page 11. Corresponding baths were made with the chloride and sulfate counter ions, as shown. Test panels of alloy 6061 and alloy 2024 were treated through standard cleaning, etching and desmutting steps and then immersed in baths containing nickel and zinc salt compositions with different counter ions (acetate, chloride and sulfate), a fluoride salt and 10 ppm of 2-MBT as the inhibitor to control any attack of the treatment chemistry on the aluminum alloy, as shown in the following table. The thus-treated panels were then electrolessly plated in an electroless nickel bath. The nickel plated

panels were checked for appearance and then for adhesion using the 90° bend test. Both inner and outer sides of the bended area were checked for peeling or flaking of the plated metal from the base substrate. Photographs showing the results of the bend tests are provided in the Exhibits B, C and D, appended to this Declaration. As clearly evident from these results, only the acetate example yielded acceptable results when plated in this process.

Bath Component	**11**	**12**	**13**
Nickel acetate•$4H_2O$	70 g/l		
Zinc acetate•$2H_2O$	30 g/l		
$ZnCl_2$, anhyd.		70 g/l	
$NiCl_2$•$6H_2O$		30 g/l	
$ZnSO_4$			70 g/l
$NiSO_4$			30 g/l
$[NH_4][HF_2]$	3 g/l	3 g/l	3 g/l
2-mercaptobenzothiazole	10 mg/l	10 mg/l	10 mg/l
pH	5.0	5.0	5.0

As shown in the Exhibit B and in the table above, solution 11, which is in accordance with the present invention, obtained good and controlled immersion deposition on the aluminum alloy substrate due to mild action of acetate based treatment chemistry. Good uniform electroless nickel deposition was obtained, with no loss of adhesion after the 90° bend test, as shown.

As shown in the Exhibit C and in the table above, solution 12, carrying out an immersion plating process using chloride salts, which is not in accordance with the present invention, did not obtain acceptable results. Due to very aggressive

action/attack on the aluminum alloy substrate, thick loose smut-like immersion deposition was obtained and caused poor deposition of electroless nickel (especially on alloy 2024). Very poor adhesion of electroless nickel was obtained, and the deposited metal layers flaked unacceptably in the 90° bend test, as shown.

As shown in the Exhibit D and in the table above, solution 13, carrying out an immersion plating process using sulfate salts, which is not in accordance with the present invention, did not obtain acceptable results. Due to the aggressive action on the aluminum alloy substrate, poor immersion deposition was obtained. Electroless nickel deposition was marginal but poor adhesion of electroless nickel was obtained, and the deposited metal layers flaked unacceptably in the 90° bend test, as shown.

(12) During the development of the presently claimed invention, it was discovered that the already-mild effects on the aluminum alloy surfaces caused by the acetate-based zinc-nickel immersion plating bath could be further reduced, and the adhesion of the zinc/nickel alloy could be further improved, by addition of the claimed mercapto-substituted heterocyclic compounds. It was discovered that the mercapto-substituted heterocyclic compounds could further inhibit the effects of treatment chemistry on the aluminum alloy surfaces, apparently by reducing the rate of aluminum metal loss from the surfaces in the slightly acidic immersion plating bath. The following compositions were prepared and tested, giving the results shown thereafter. In all cases, the solution pH = 5.5.

As shown by the results in the following table, consistently good results in both aluminum alloys were obtained with the mercapto-substituted inhibitor compounds, while less favorable, not acceptable results were obtained with the other additives or with no additive.

Bath Component	1	2	3	4	5	6	7	Control
Nickel acetate•$4H_2O$	70 g/l	70 g/l	70 g/l	70 g/l	70 g/l	70 g/l	70 g/l	70 g/l
Zinc acetate•$2H_2O$	30 g/l	30 g/l	30 g/l	30 g/l	30 g/l	30 g/l	30 g/l	30 g/l
$[NH_4][HF_2]$	3 g/l	3 g/l	3 g/l	3 g/l	3 g/l	3 g/l	3 g/l	3 g/l
2-mercaptobenzothiazole	10 mg/l	-	-	-	-	-	-	-
2,2'-dipyridyl	-	10 mg/l	-	-	-	-		-
1,3-diethyl-2-thiourea	-	-	10 mg/l	-	-	-	-	-
2-benzimidazolethiol	-	-	-	10 mg/l	-	-	-	-
2-mercapto-1-methylimidazole	-	-	-	-	10 mg/l	-	-	-
1,10-phenanthroline	-	-	-	-	-	10 mg/l	-	-
sodium thiocyanate	-	-	-	-	-	-	10 mg/l	-
RESULTS:								
6061 Adhesion	good	fair	good	good	good	fair	poor	fair
2042 Adhesion	good	good	good	good	good	good	good	good

(13) Similar results from acetate and the claimed inhibitors are included in Tables I, II and III in the present application.

(14) In preparation of the present Declaration, Applicants have conducted comparative testing to show that the claimed pH range, from a pH from about 4.5 to about 5.5, is important and provides an additional distinction over the prior art. Test panels of alloy 6061 and alloy 2024 were treated through standard cleaning, etching and desmutting steps and then immersed in baths containing nickel and zinc acetate, a fluoride salt and 10 ppm of 2-MBT as the inhibitor to control any attack of the treatment chemistry on the aluminum alloy, and the pH was adjusted to 4.0, 5.0 or 6.0, as shown in the following table. The thus-treated panels were then electrolessly plated in an electroless nickel bath. The nickel plated panels were checked for appearance and then for adhesion using the 90° bend test. Both inner and outer sides of the bended areas were checked for peeling or flaking of the plated metal from the base substrate.

Bath Component	**11**	**11a**	**11b**
Nickel acetate•$4H_2O$	70 g/l	70 g/l	70 g/l
Zinc acetate•$2H_2O$	30 g/l	30 g/l	30 g/l
$ZnCl_2$, anhyd.			
$NiCl_2$•$6H_2O$			
$ZnSO_4$			
$NiSO_4$			
$[NH_4][HF_2]$	3 g/l	3 g/l	3 g/l
2-mercaptobenzothiazole	10 mg/l	10 mg/l	10 mg/l
pH	5.0	4.0	6.0

Photographs showing the results of the bend tests are provided in the Exhibits E, F and G, appended to this Declaration. As clearly evident from these results, only the pH 5.0 example yielded acceptable results when plated in this process. As shown in the table, the only difference between Baths 11, 11a and 11b is the pH. As shown in the photograph in Exhibit E, at pH 4.0, there is clearly poor adhesion and flaking of the electroless nickel deposit. As shown in the photograph at Exhibit F, at pH 5.0 there is good adhesion and no flaking of the electroless nickel deposit. As shown in the photograph at Exhibit G, at pH 6.0, there is good adhesion and no apparent flaking of the electroless nickel deposit, but the deposit is not as good as at pH 5.0 and is only borderline acceptable. Although not shown here, at slightly higher pH, e.g., at about pH 6.5, the deposit becomes unacceptable. Thus, it is demonstrated that the pH limits are important elements of the claimed invention, and do provide an important distinction over the lower pH prior art, such as the pH of JP '864, and certainly better than the lower pH of the Heiman reference.

(15) The following conclusions can be drawn from the foregoing test results.

A. First, as shown by both the data in the application and the recently-obtained data presented above, use of the acetate salts of the metal ions provides an unexpected and significant benefit, when used together with the other elements of the presently claimed invention. As shown by these results, the acetate, in combination with the specified inhibitors and with the mildly acidic pH, all of which are specified in the claims of our present application, provides an excellent protective coating on the aluminum or aluminum alloy surfaces, which facilitates subsequent application of a thicker layer such as the electroless nickel that results in a superior product, as shown by the 90° bend test results.

B. Second, it is clear that the mercapto-substituted heterocyclic compounds provide a much improved performance compared to other additives. These other

additives that provide inferior performance in these tests are also known as brighteners in electroplating processes. This shows that just because a given compound may be known for use as an electroplating brightener, there is no reason or basis to expect that it would work either for the purpose of our present invention or as a brightener in any immersion plating process.

C. Third, it is clear that the selection of a chemical composition for use as a zincate replacement is not a simple matter of selecting any superficially similar prior art composition and arbitrarily modifying it, as the Examiner apparently contends, which contention I understand to be the basis for the rejections of the claims of our present application. To the contrary, our invention is the result of a research and development program by which we have developed a very fine balance of the chemistry to control both the aluminum etch rate and the zinc/nickel deposition rate during the immersion process of depositing a very thin, well controlled layer of the zinc and nickel alloy onto the aluminum substrate. The process requires a controlled amount of acidity, which is very low (i.e., pH from about 4.5 to about 5.5), along with the specific inhibitor to control the dissolution rate of the substrate aluminum.

D. Fourth, as shown by the test results, the pH of the immersion bath of the present invention, i.e., pH from about 4.5 to about 5.5, is very important, and there is nothing in the prior art to suggest that this pH range would have any particular effect.

E. Finally, contrary to the Examiner's contentions, the inhibitor of our present invention is used for the purpose of inhibiting dissolution of aluminum from the substrate, and for controlling the rate of zinc/nickel deposition, not for the purpose of brightening the deposit. The zinc alloy deposit obtained by the present invention is so thin that there would be no point and no benefit expected or actually obtained by use a brightener of any kind. Accordingly, with all due respect to the Examiner's education, training and experience, it is my considered opinion as a person of skill in the art that the Examiner is mistaken in contending or concluding that the present invention would

have been obvious to any person of ordinary skill in the art at the time the invention was made, based on the reasoning that has been set forth in the Office Actions during the prosecution of our present application.

I, Nayan H. Joshi, hereby declare that all statements made herein of my own knowledge are true and that all statements made on information and belief are believed to be true; and further that these statements were made with knowledge that willful false statements and the like are punishable by fine or imprisonment, or both, under Section 1001 of Title 18 of the United States Code, and that such willful false statements may jeopardize the validity of the application or any patent issued therefrom.

Respectfully submitted,

4-28-08
Date

N. Joshi
Nayan H. Joshi

Journal of The Electrochemical Society, **150** (9) C591-C599 (2003)
0013-4651/2003/150(9)/C591/9/$7.00 © The Electrochemical Society, Inc.

A Mechanism for Brightening

Linear Stability Analysis of the Curvature-Enhanced Coverage Model

G. B. McFadden,[z] S. R. Coriell, T. P. Moffat,* D. Josell, D. Wheeler, W. Schwarzacher,* and J. Mallett

National Institute of Standards and Technology, Gaithersburg, Maryland 20899-8910, USA

This work presents experiments and theory describing a mechanism for how brighteners in electrolytes function. The mechanism involves change of local coverage of a deposition rate-enhancing catalyst adsorbed on the surface through change of local surface area during growth as well as accumulation and consumption. A first-order perturbation analysis shows the surface is stable against growth of perturbations for all wavelengths below a critical value that is deposition-condition dependent. The model predictions are shown to be consistent with the experimental results.

Manuscript submitted September 18, 2002; revised manuscript received March 3, 2003. Available electronically July 24, 2003.

Roughness evolution during electrodeposition is a subject of wide-ranging scientific and technical interest. Experience has shown that metal ion depletion at the interface is usually associated with destabilization of planar growth fronts. This has been explained by Mullins-Sekerka morphological stability theory which examines system response to small perturbations from steady-state growth conditions. Typically, a sinusoidal variation of surface height is imposed on the flat surface, and the resulting time evolution, to first order in the amplitude of the perturbation, is analyzed.[1,2] A positive growth rate reflects instability while a negative value results in attenuation of the perturbation; the former yields a rough surface while the latter case gives a smooth interface. This type of analysis has been widely applied to study phase transformations ranging from solidification,[1,2] to additive-free electroplating,[3-11] and chemical vapor deposition.[12,13] In contrast to the destabilizing influence of the reactant gradient, it is known that capillarity, adatom diffusion, and reaction kinetics dampen, and even stabilize the system, particularly at shorter wavelengths.

An important aspect of electroplating practice involves the use of electrolyte additives to generate smooth, optically bright films. In certain instances, additives even allow the leveling of undesired surface imperfections by inducing preferential deposition at the bottom of features such as scratches. The traditional leveling mechanism behind this process is the existence of a concentration gradient of the inhibiting additive that results in lower deposition of the inhibitor, with associated decreasing inhibition of the metal deposition, the farther down one goes in the defect.[14-17] It is generally known that electrolytes that otherwise deposit at equal rates on all surfaces can be induced to deposit preferentially at the bottoms of polishing scratches and other surface imperfections through the addition of deposition-rate inhibiting additives.

It is generally recognized that the traditional leveling mechanism will not affect deposition substantially when the dimensions of the defect are orders of magnitude smaller than the thickness of the boundary layer responsible for the concentration gradient. For optically relevant dimensions that are only a fraction of 1 μm and a typical boundary layer thickness of 100 μm, the appropriateness of such a model becomes questionable. For this reason, electrolytes commonly used for industrial plating applications that require optically bright deposits typically contain a variety of additives that have been empirically determined to yield bright deposits. There is no fundamental basis for determining which additives to add or why.

Recent publications have detailed a mechanism for the superconformal deposition process now used to achieve bottom-to-top filling of submicrometer dimension features. The mechanism involves (*i*) the adsorption of a deposition-rate enhancing catalyst on the deposit surface and (*ii*) changes in the local catalyst coverage induced by the changing surface area on regions with nonzero curvature.[18,19] Models based on this curvature enhanced accelerator coverage (CEAC) mechanism yield predictions of superconformal filling of fine features due to the increase of catalyst coverage during deposition on the concave bottom surfaces of filling features.[18-22] The implications for brightening of a mechanism that increases deposition rates at the bottoms of valleys (concave surfaces) while slowing deposition on the tops of hills (convex surfaces) have been noted. This mechanism has also been shown to describe superconformal feature filling by surfactant catalyzed chemical vapor deposition (CVD) of copper.[23]

This work presents a linear stability analysis to establish just how such a mechanism would stabilize a surface against roughening as well as determining the parameters and conditions for which such a mechanism will function optimally. An infinitesimal sinusoidal perturbation of the surface height and catalyst coverage is imposed on the flat surface, and the resulting time evolution to the first order in the amplitude of the perturbation is analyzed. In the tradition of morphological stability analyses, the real part of the complex exponent that describes the time dependence of the perturbation amplitude determines the stability of the surface. A positive value indicates growth of the instability while a negative value results in attenuation.

Governing Equations

We consider electrodeposition of copper from an aqueous solution containing copper ions of concentration C_c and a catalyst (accelerator) of concentration C_a in the presence of an overvoltage η. We assume that growth of solid copper occurs at constant velocity V in the z direction. Diffusion equations in the solution for C_c and the catalyst C_a are written in a reference frame moving with this constant velocity

$$\frac{\partial C_c}{\partial t} - V\frac{\partial C_c}{\partial z} = D_c\nabla^2 C_c \qquad [1]$$

$$\frac{\partial C_a}{\partial t} - V\frac{\partial C_a}{\partial z} = D_a\nabla^2 C_a \qquad [2]$$

where t is time, and the constants D_c and D_a are the diffusion coefficients for C_c and C_a, respectively. The mean position of the liquid-solid interface is assumed to be $z = 0$. Far-field boundary conditions in the solution are applied at the edge of a boundary layer at $z = \delta$

$$C_c = C_c^\infty \quad C_a = C_a^\infty \qquad [3]$$

The catalyst is adsorbed on the solid-liquid interface and has a saturation coverage Γ_0. The fractional catalyst coverage is described by

* Electrochemical Society Active Member.
[z] E-mail: mcfadden@nist.gov

a dimensionless parameter θ, defined so that $\Gamma_0\theta$ is the local interface coverage in units of moles per unit area. The coverage is governed by

$$\frac{d\theta}{dt} = k^+(1-\theta)C_a - k^-\theta^n + v_N\mathcal{K}\theta \quad [4]$$

where $v_N = (V + h_t)/\sqrt{1+h_x^2}$ is the normal velocity of the interface $z = h(x,t)$, $\mathcal{K} = h_{xx}/[1+h_x^2]^{3/2}$ is the mean curvature of the interface, and the exponent n is a constant. Here we have assumed a two-dimensional interface for notational simplicity, but the results can be immediately applied to a general three-dimensional interface. Our sign convention is such that the curvature of a solid sphere is negative. The parameters k^+ and k^- describe the adsorption and desorption of the catalyst at the interface and depend on the overvoltage η. We use the specific forms

$$k^+ = 230\exp(-f\eta/2) \quad [\mathrm{cm^3/mol\ s}] \quad [5]$$

$$k^- = -0.08\eta + \frac{1.1}{\exp(-35[\eta+0.098]) + \exp(45[\eta+0.098])}[\mathrm{s^{-1}}] \quad [6]$$

where $f = \mathcal{F}/RT$, $\mathcal{F}$ is Faraday's constant, R is the ideal gas constant, and T is the temperature; here η is measured in volts. The values used approximate the kinetics for an electrolyte that is described later. The particular forms of the voltage dependence have no bearing on the nature of the stabilization problem beyond the values of k^+ and k^- that they yield.

Flux conditions at the interface are given by

$$D_c\frac{\partial C_c}{\partial \mathbf{N}} = -v_N(C_c - V_c) \quad [7]$$

$$D_a\frac{\partial C_a}{\partial \mathbf{N}} = \Gamma_0 k^+(1-\theta)C_a \quad [8]$$

where $V_c = 1/\Omega$, Ω is the molar volume of solid copper, and $\mathbf{N}$ is the normal vector to the interface. In writing Eq. 8 we have neglected a term of the form $v_N C_a$ that is expected to be small compared to the other terms. We have also assumed that there is no desorption of the strongly adsorbing catalyst from the surface of the solid; rather the $k^-\theta^n$ loss term in Eq. 4 represents either incorporation (trapping) of catalyst within the solid, where it has no effect on deposition, and/or desorption of an inactivated part of the catalyst molecule.

The normal velocity satisfies the relation

$$v_N = \frac{i\Omega}{2\mathcal{F}} \quad [9]$$

where the current i is given by the Butler-Volmer equation

$$i = i_0(\theta)\frac{C_c}{C_c^\infty}\exp\left\{-\alpha(\theta)\left[\frac{\mathcal{F}\eta - \Omega\gamma\mathcal{K}}{RT}\right]\right\} \quad [10]$$

we have neglected the current due to the reverse reaction. Here γ is the free energy of the solid-liquid interface. We use a model with

$$i_0(\theta) = b_0 + b_1\theta \quad [11]$$

$$\alpha(\theta) = m_0 + m_1\theta \quad [12]$$

values for the constants b_0, b_1, m_0, and m_1 that we use are also given in Table I.

Table I. Thermophysical properties used in calculations.

Bulk concentration of cupric ion	C_c^∞	2.78×10^{-4}	mol/cm^3
Diffusion coefficient for catalyst	D_a	5.6×10^{-6}	cm^2/s
Diffusion coefficient for cupric ion	D_c	5.6×10^{-6}	cm^2/s
Faraday constant	$\mathcal{F}$	96,485	C/mol
Ideal gas constant	R	8.314	J/K mol
Temperature	T	298	K
Surface energy	γ	1.952×10^{-4}	J/cm^2
Saturation surface coverage	Γ_0	0.635×10^{-9}	mol/cm^2
Thickness of hydrodynamic boundary layer	δ	0.0156	cm
Molar volume of copper	Ω	7.1	cm^3/mol
Exchange current density	b_0	0.026×10^{-3}	A/cm^2
coverage dependence	b_1	4.5×10^{-3}	A/cm^2
Metal deposition transfer coefficient	m_0	0.5	
coverage dependence	m_1	0.0	
Coverage exponent	n	3	

Base State

The stability of the system is considered by perturbing an initially planar interface and determining whether the perturbations grow or decay in time. The perturbed quantities, assumed to be small, are denoted by a superscript (1) and the unperturbed base state is denoted by a superscript (0).

The base state satisfies

$$k^+(1-\theta^{(0)})C_a^I - k^-[\theta^{(0)}]^n = 0 \quad [13]$$

$$C_c^{(0)}(z) = C_c^I + (C_c^\infty - C_c^I)\frac{[1-\exp(-zV/D_c)]}{[1-\exp(-\delta V/D_c)]} \quad [14]$$

$$C_a^{(0)}(z) = C_a^I + (C_a^\infty - C_a^I)\frac{[1-\exp(-zV/D_a)]}{[1-\exp(-\delta V/D_a)]} \quad [15]$$

where $C_c^I = C_c^{(0)}(z=0)$ and $C_a^I = C_a^{(0)}(z=0)$ denote the concentrations at the planar interface. We denote the unperturbed solute gradients at the planar interface by

$$G_c = \frac{dC_c^{(0)}}{dz}(z=0) = \frac{-V(C_c^I - V_c)}{D_c} \quad [16]$$

$$G_a = \frac{dC_a^{(0)}}{dz}(z=0) = \frac{\Gamma_0 k^+(1-\theta^{(0)})C_a^I}{D_a} \quad [17]$$

By substituting the concentration fields given by Eq. 14 and 15 into the flux conditions in Eq. 7 and 8 we obtain

$$C_c^I = V_c + (C_c^\infty - V_c)\exp(\delta V/D_c) \quad [18]$$

$$C_a^I = \frac{VC_a^\infty}{V + \Gamma_0 k^+(1-\theta^{(0)})[1-\exp(-\delta V/D_a)]} \quad [19]$$

The unperturbed interface velocity is given by

$$V = \frac{i_0(\theta^{(0)})\Omega C_c^I}{2\mathcal{F}C_c^\infty}\exp\left[\frac{-\alpha(\theta^{(0)})\mathcal{F}\eta}{RT}\right] \quad [20]$$

We note that for $\delta V/D_c \ll 1$ and $\delta V/D_a \ll 1$, we may approximate the exponentials in Eq. 19 and 18 to obtain

$$C_a^I = \frac{C_a^\infty}{1 + \Gamma_0 k^+(1-\theta^{(0)})\delta/D_a} \quad [21]$$

and

$$C_c^I = C_c^\infty + (C_c^\infty - V_c)\delta V/D_c \quad [22]$$

The four unknowns C_a^I, C_c^I, V, and $\theta^{(0)}$ are determined by Eq. 13, 18, 19 and 20. These nonlinear equations are solved numerically to determine the base state.

Perturbed System

We perturb the system by writing

$$\begin{pmatrix} C_c(x,z,t) \\ C_a(x,z,t) \\ \theta(x,t) \\ h(x,t) \end{pmatrix} = \begin{pmatrix} C_c^{(0)}(z) \\ C_a^{(0)}(z) \\ \theta^{(0)} \\ 0 \end{pmatrix} + \exp(\sigma t + i\omega x) \begin{pmatrix} C_c^{(1)}(z) \\ C_a^{(1)}(z) \\ \hat{\theta} \\ \hat{h} \end{pmatrix} + \ldots \quad [23]$$

where σ is the temporal growth rate of the perturbation amplitudes and ω is the wavenumber of the sinusoidal interface perturbation. The wavelength of the perturbation is given by $\lambda = 2\pi/\omega$.

The perturbed concentration fields are given by

$$C_j^{(1)}(z) = \hat{C}_j \frac{\exp(-Vz/2D_j)[\exp(-R_j z) - \exp(R_j z)\exp(-2R_j\delta)]}{1 - \exp(-2R_j\delta)} \quad [24]$$

for $j = c$ and $j = a$, with

$$R_j = \sqrt{\left(\frac{V}{2D_j}\right)^2 + \frac{\sigma}{D_j} + \omega^2} \quad [25]$$

The perturbed flux conditions are obtained by linearizing the boundary conditions given by Eq. 7 and 8 and inserting the perturbed concentration fields given from Eq. 24. The linearized boundary conditions are applied at $z = 0$, and are obtained by taking into account the variations associated with both the perturbed concentration fields and the perturbed interface height. Specifically, a general function $f(x,z,t) = f^{(0)}(z) + f^{(1)}(x,z,t) + \ldots$ evaluated at the perturbed interface position $z = h^{(1)}(x,t)$ has the expansion

$$f[x,h^{(1)}(x,t),t] \approx f^{(0)}[h^{(1)}(x,t)] + f^{(1)}[x,h^{(1)}(x,t),t] + \ldots \approx f^{(0)}(0) + \left\{f^{(1)}(x,0,t) + \frac{df^{(0)}}{dz}(0)h^{(1)}(x,t)\right\} + \ldots \quad [26]$$

through first order in the perturbation amplitudes. This type of expansion applies to the interface concentrations and also to their normal derivatives, since to first order the normal derivative is equal to the derivative with respect to z. For the boundary conditions given by Eq. 7 and 8 this procedure results in the expressions

$$-D_c\frac{[(R_c + V/2D_c) + (R_c - V/2D_c)\exp(-2R_c\delta)]}{[1 - \exp(-2R_c\delta)]}\hat{C}_c = -\sigma\hat{h}[C_c^I - V_c] - V\hat{C}_c \quad [27]$$

and

$$B_a\hat{C}_a + D_a\frac{d^2C_a^{(0)}}{dz^2}(z = 0)\hat{h} = -\Gamma_0 k^+ C_a^I\hat{\theta} + \Gamma_0 k^+(1 - \theta^{(0)}) \times[\hat{C}_a + G_a\hat{h}] \quad [28]$$

where

$$B_a = -D_a\frac{[(R_a + V/2D_a) + (R_a - V/2D_a)\exp(-2R_a\delta)]}{[1 - \exp(-2R_a\delta)]} \quad [29]$$

Linearizing the Butler-Volmer equation gives

$$\left(\frac{\sigma}{V}\right)\hat{h} = \left[\frac{i_0'(\theta^{(0)})}{i_0(\theta^{(0)})} - \frac{\mathcal{F}\eta}{RT}\alpha'(\theta^{(0)})\right]\hat{\theta} + \left[\frac{G_c}{C_c^I} - \frac{\alpha(\theta^{(0)})\Omega\gamma\omega^2}{RT}\right]\hat{h} + \frac{1}{C_c^I}\hat{C}_c \quad [30]$$

The linearized coverage equation is

$$\sigma\hat{\theta} = k^+(1 - \theta^{(0)})[\hat{C}_a + G_a\hat{h}] - k^+C_a^I\hat{\theta} - n[\theta^{(0)}]^{n-1}k^-\hat{\theta} - V\theta^{(0)}\omega^2\hat{h} \quad [31]$$

Dispersion Relation

To derive the dispersion relation, we first eliminate $\hat{C}_c$ from Eq. 27 to obtain

$$\hat{C}_c = \sigma A\hat{h} \quad [32]$$

where

$$A = \frac{[1 - \exp(-2R_c\delta)]G_c/V}{[(V/2D_C - R_c) - (V/2D_C + R_c)\exp(-2R_c\delta)]} \quad [33]$$

Next, using $C_a^{(0)}(z)$ from Eq. 15 and the definition of G_a from Eq. 17, Eq. 28 gives

$$0 = [\Gamma_0 k^+(1 - \theta^{(0)}) - B_a]\hat{C}_a + G_a[\Gamma_0 k^+(1 - \theta^{(0)}) + V]\hat{h} - \Gamma_0 k^+ C_a^I\hat{\theta} \quad [34]$$

Then, from Eq. 30 and 32 we have

$$0 = VF\hat{\theta} + \left[\frac{VG_c}{C_c^I} - \frac{\alpha(\theta^{(0)})\Omega V\gamma\omega^2}{RT} + \frac{V\sigma A}{C_c^I} - \sigma\right]\hat{h} \quad [35]$$

where

$$F = \frac{i_0'(\theta^{(0)})}{i_0(\theta^{(0)})} - \frac{\mathcal{F}\eta}{RT}\alpha'(\theta^{(0)}) \quad [36]$$

Finally, Eq. 31 can be rewritten

$$0 = [k^+(1 - \theta^{(0)})]\hat{C}_a - [\sigma + k^+C_a^I + n[\theta^{(0)}]^{n-1}k^-]\hat{\theta} + [G_a k^+(1 - \theta^{(0)}) - V\theta^{(0)}\omega^2]\hat{h} \quad [37]$$

Equations 32, 34, 35, and 37 constitute four homogeneous linear equations in the variables $\hat{C}_c$, $\hat{C}_a$, $\hat{h}$, and $\hat{\theta}$. Setting the determinant of the linear system to zero provides a dispersion relation of the form

$$-B_a\Big\{VF[G_a k^+(1-\theta^{(0)}) - V\theta^{(0)}\omega^2] + (\sigma + k^+C_a^I + n[\theta^{(0)}]^{n-1}k^-)\Big(\frac{VG_c}{C_c^I} - \frac{\alpha[\theta^{(0)}]\Omega V\gamma\omega^2}{RT} + \frac{V\sigma A}{C_c^I} - \sigma\Big)\Big\} + k^+(1-\theta^{(0)})\Big\{\Gamma_0(\sigma + n[\theta^{(0)}]^{n-1}k^-) \times\Big(\frac{VG_c}{C_c^I} - \frac{\alpha(\theta^{(0)})\Omega V\gamma\omega^2}{RT} + \frac{V\sigma A}{C_c^I} - \sigma\Big) - \Gamma_0 V^2 F\theta^{(0)}\omega^2 - V^2 FG_a\Big\} = 0 \quad [38]$$

Approximate Solution for Large ω

If we assume that ω is large enough that the square of the wavenumber dominates both $(V/2D_j)^2$ and $|\sigma|/D_j$ then $R_j \approx \omega$. If we further assume that $\delta\omega \gg 1$, then $B_a \approx -D_a\omega$ and $A \approx -G_c/(V\omega)$. Thus the term proportional to B_a dominates the dispersion relation Eq. 38, and neglecting A gives the approximate dispersion relation

$$VF[G_a k^+(1-\theta^{(0)}) - V\theta^{(0)}\omega^2] + (\sigma + k^+C_a^I + n[\theta^{(0)}]^{n-1}k^-) \times\Big(\frac{VG_c}{C_c^I} - \frac{\alpha(\theta^{(0)})\Omega V\gamma\omega^2}{RT} - \sigma\Big) = 0 \quad [39]$$

or

$$\sigma^2 + \Big[k^+C_a^I + n[\theta^{(0)}]^{n-1}k^- - \frac{VG_c}{C_c^I} + \frac{\alpha(\theta^{(0)})\Omega V\gamma\omega^2}{RT}\Big]\sigma - VF[G_a k^+(1-\theta^{(0)}) - V\theta^{(0)}\omega^2] - [k^+C_a^I + n[\theta^{(0)}]^{n-1}k^-]\Big(\frac{VG_c}{C_c^I} - \frac{\alpha(\theta^{(0)})\Omega V\gamma\omega^2}{RT}\Big) = 0 \quad [40]$$

We note that in the exact dispersion relation Eq. 38, A only appears as the product σA. At an onset of instability with $\sigma = 0$ (real mode), A therefore has no effect on the critical wavenumber. We find that the complex modes with $\sigma_i \neq 0$ have large critical wavenumbers, so that A is negligible for these modes as well.

Equation 40 is the same dispersion relation that is obtained by linearizing the system

$$\frac{d\theta}{dt} = k^+(1-\theta)C_a - k^-\theta^n + v_n\mathcal{K}\theta \quad [41]$$

$$v_n = i_0(\theta)\frac{\Omega C_c}{2\mathcal{F}C_c^\infty}\exp\Big\{-\alpha(\theta)\Big[\frac{\mathcal{F}\eta - \Omega\gamma\mathcal{K}}{RT}\Big]\Big\} \quad [42]$$

both evaluated at the interface, with the concentration fields given by

$$C_c(z) = C_c^I + G_c z \quad [43]$$

$$C_a(z) = C_a^I + G_a z \quad [44]$$

The values of C_c^I and C_a^I depend on δ and are obtained from the full expressions in Eq. 18 and 19. In other words, the linearized system obtained from Eq. 41 and 42

$$\sigma\hat{\theta} = k^+[1-\theta^{(0)}]G_a\hat{h} - (k^+C_a^I + n[\theta^{(0)}]^{n-1}k^-)\hat{\theta} - V\theta^{(0)}\omega^2\hat{h} \quad [45]$$

$$\sigma\hat{h} = \Big[\frac{VG_c}{C_c^I} - \frac{\alpha(\theta^{(0)})\Omega V\gamma\omega^2}{RT}\Big]\hat{h} + VF\hat{\theta} \quad [46]$$

also has the dispersion relation given by Eq. 40. Essentially, these small wavelength perturbations only sample, without affecting, the gradients in the concentration fields immediately adjacent to the interface.

If we ignore the coupling between $\hat{\theta}$ and $\hat{h}$ in Eq. 45 by neglecting the terms proportional to $\hat{h}$, this equation represents a stable real mode with $\sigma = -(k^+C_a^I + n[\theta^{(0)}]^{n-1}k^-)$. Similarly, if we neglect the term proportional to $\hat{\theta}$ in Eq. 46, this equation represents a real mode with $\sigma = VG_c/C_c^I - \alpha(\theta^{(0)})\Omega V\gamma\omega^2/RT$. The concentration gradient G_c is destabilizing, and the surface tension γ is stabilizing; the mode is unstable for small ω and stable for large ω. With the coupling included in these equations the situation is more complicated and, still assuming the modes are real, depends on the relative phase between $\hat{\theta}$ and $\hat{h}$. For example, if they are in phase, with $\hat{\theta}/\hat{h} > 0$, the positive term VF in Eq. 46 is destabilizing and is stabilizing if they are out of phase, with $\hat{\theta}/\hat{h} < 0$. For Eq. 45, the coupling depends on the sign of the term $k^+[1-\theta^{(0)}]G_a - V\theta^{(0)}\omega^2$, which is positive for small ω and negative for large ω. When this term is negative, the mode is stabilized if $\hat{\theta}$ and $\hat{h}$ are in phase, and destabilized if they are out of phase. The relative phase of $\hat{\theta}$ and $\hat{h}$ are determined by examining the linearized boundary conditions once σ has been determined. In many cases, at the onset of instability they are found to be out of phase. In the limit of large wavenumbers, the perturbed interfacial concentrations $\hat{C}_c$ and $\hat{C}_a$ both vanish to leading order. More generally, at the onset of instability for a real mode ($\sigma = 0$) Eq. 32 shows that the relative phase between $\hat{C}_c$ and $\hat{h}$ changes from being in phase to being out of phase as the growth rate passes through zero.

The solution to the approximate dispersion relation in Eq. 40 can be written in the form

$$\sigma = \frac{1}{2}\Big(\frac{VG_c}{C_a^I} - \frac{\alpha(\theta^{(0)})\Omega V\gamma\omega^2}{RT} - k^+C_a^I - n[\theta^{(0)}]^{n-1}k^-\Big) \pm \sqrt{\frac{1}{4}\Big(\frac{VG_c}{C_c^I} - \frac{\alpha(\theta^{(0)})\Omega V\gamma\omega^2}{RT} + k^+C_a^I + n[\theta^{(0)}]^{n-1}k^-\Big)^2 + VFG_a k^+(1-\theta^{(0)}) - V^2F\theta^{(0)}\omega^2} \quad [47]$$

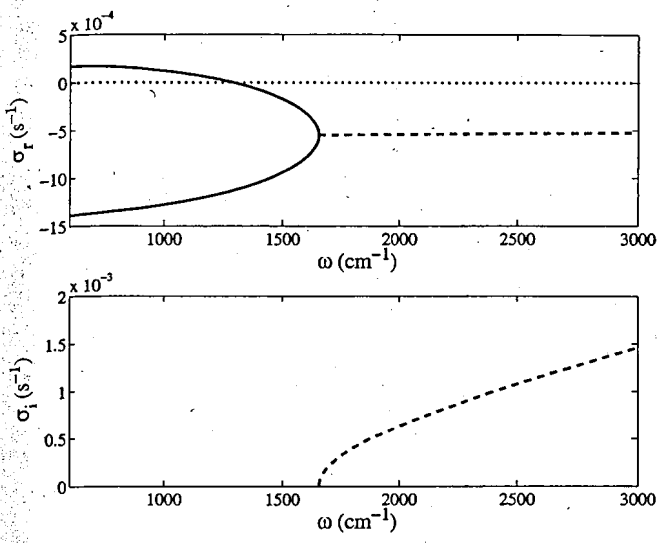

Figure 1. The real and imaginary parts of the temporal growth rate σ as a function of the wavenumber ω of a sinusoidal perturbation for $\eta = -0.3$ V and $C_a^\infty = 1.0 \times 10^{-9}$ mol/cm^3. The axis $\sigma_r = 0$ is indicated by the dotted line.

The stability criterion for a quadratic of the form

$$\sigma^2 + a_1\sigma + a_2 = 0 \qquad [48]$$

is (see Ref. 24)

$$a_1 \geq 0 \quad a_2 \geq 0 \qquad [49]$$

if either of these conditions is violated the solution is unstable. For our system, the condition $a_1 > 0$ yields

$$\left[\frac{\alpha(\theta^{(0)})\Omega V\gamma}{RT}\right]\omega^2 \geq \frac{VG_c}{C_c^I} - k^+C_a^I - n[\theta^{(0)}]^{n-1}k^- \qquad [50]$$

while the condition $a_2 > 0$ yields

$$\left[VF\theta^{(0)} + \left(\frac{\alpha(\theta^{(0)})\Omega\gamma}{RT}\right)(k^+C_a^I + n[\theta^{(0)}]^{n-1}k^-)\right]\omega^2 \geq F[G_ak^+(1-\theta^{(0)})] + \left[\frac{G_c}{C_c^I}\right](k^+C_a^I + n[\theta^{(0)}]^{n-1}k^-) \qquad [51]$$

The surface tension term in Eq. 50 guarantees that this inequality is satisfied for sufficiently large ω. For sufficiently large values of C_a^I the right side of Eq. 50 is negative, and stability is then determined by Eq. 51. In Eq. 51, the term $(G_c/C_c^I)(k^+C_a^I + n[\theta^{(0)}]^{n-1}k^-)$ usually dominates the right side. On the left side, the term $VF\theta^{(0)}$ usually dominates the second term, proportional to $\alpha(\theta^{(0)})\Omega\gamma/RT$, and hence the effects of surface tension are negligible. We next consider this limit.

Zero surface free energy limit (γ=0).—We first consider the simplified case in which we neglect the effects of surface-free energy.

In that case, for large ω, such that

$$V^2F\theta^{(0)}\omega^2 > \frac{1}{4}\left(\frac{VG_c}{C_c^I} + k^+C_a^I + n[\theta^{(0)}]^{n-1}k^-\right)^2 + VFG_ak^+(1-\theta^{(0)}) \qquad [52]$$

a purely imaginary value is obtained for the radical in Eq. 47. Stability is therefore determined only by the sign of the term outside the radical, *i.e.*,

$$Re[\sigma] = \frac{1}{2}\left(\frac{VG_c}{2C_c^I} - k^+C_a^I - n[\theta^{(0)}]^{n-1}k^-\right) \qquad [53]$$

We therefore have stability if

$$k^+C_a^I + n[\theta^{(0)}]^{n-1}k^- > \frac{VG_c}{C_c^I} \qquad [54]$$

On the other extreme, for small ω, we have

$$\frac{1}{4}\left(\frac{VG_c}{C_c^I} + k^+C_a^I + n[\theta^{(0)}]^{n-1}k^-\right)^2 + VFG_ak^+(1-\theta^{(0)}) - V^2F\theta^{(0)}\omega^2 > 0 \qquad [55]$$

so that a real value is obtained for the radical in Eq. 47, resulting in two real roots. In addition, since

$$VFG_ak^+(1-\theta^{(0)}) + \frac{VG_c}{C_c^I}(k^+C_a^I + n[\theta^{(0)}]^{n-1}k^-) > 0 \qquad [56]$$

the radical is the dominant term in Eq. 47, and there is one stable and one unstable root for small enough ω. (But we emphasize that this discussion applies to the approximate dispersion relation which was obtained in a large ω limit.) If Eq. 54 holds, the unstable root is stabilized for increasing ω by the term $V^2F\theta^{(0)}\omega^2$, and is neutrally stable at the marginal wavenumber given by

$$VF\theta^{(0)}\omega^2 = FG_ak^+(1-\theta^{(0)}) + \frac{G_c}{C_c^I}(k^+C_a^I + n[\theta^{(0)}]^{n-1}k^-) \qquad [57]$$

When ω further increases to the value

Table II. Numerical results for $C_c^\infty = 2.78 \times 10^{-4}$ mol/cm^3 and $\eta = -0.3$ V.

C_a^∞ (mol/cm^3)	C_a^I (mol/cm^3)	$10^5\ C_c^I$ (mol/cm^3)	$\theta^{(0)}$	10^7 V (cm/s)	ω_c (cm^{-1})	σ_i (s^{-1})
1.0×10^{-7}	9.37×10^{-8}	0.640	0.522	6.93	10452	0
1.0×10^{-8}	9.08×10^{-9}	1.178	0.275	6.79	3730.3	0
1.0×10^{-9}	8.92×10^{-10}	2.260	0.135	6.52	1289.9	0
1.0×10^{-10}	8.84×10^{-11}	4.205	0.0641	6.02	453.87	0
1.0×10^{-11}	8.80×10^{-12}	7.168	0.0300	5.27	13810	6.61×10^{-3}
1.0×10^{-12}	8.79×10^{-13}	10.73	0.0140	4.36	15579	5.69×10^{-3}
1.0×10^{-13}	8.78×10^{-14}	13.99	0.00652	3.53	13931	3.57×10^{-3}
1.0×10^{-14}	8.78×10^{-15}	16.28	0.00303	2.94	12402	2.13×10^{-3}

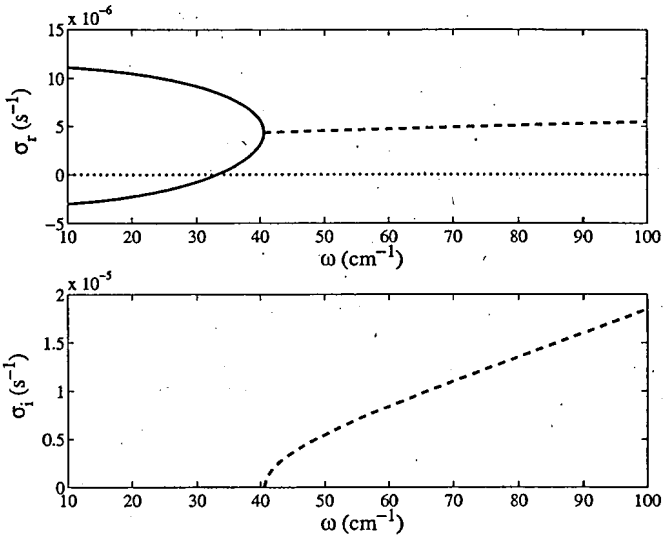

Figure 2. The real and imaginary parts of the temporal growth rate σ as a function of the wavenumber ω of a sinusoidal perturbation for $\eta = -0.3$ V and $C_a^\infty = 1.0 \times 10^{-13}$ mol/cm^3. The axis $\sigma_r = 0$ is indicated by the dotted line.

$$V^2F\theta^{(0)}\omega^2 = \frac{1}{4}\left(\frac{VG_c}{C_c^I} + k^+C_a^I + n[\theta^{(0)}]^{n-1}k^-\right)^2 + VFG_ak^+[1 - \theta^{(0)}] \qquad [58]$$

the two real modes coincide, and for larger ω we obtain a pair of stable complex conjugate modes.

The limit of vanishing catalyst concentration.—If there is no catalyst present in the electrolyte, $C_a^\infty = 0$, then the coverage $\theta^{(0)}$ also vanishes and the dispersion Relation 47 reduces to

$$\frac{\sigma}{V} = \frac{G_c}{C_c^I} - \frac{m_0\Omega\gamma\omega^2}{RT} \qquad [59]$$

Because the copper concentration in the solid is much higher than that in the liquid, $V_c \gg C_c^I$, Eq. 16 and 20 yield

$$\frac{G_c}{C_c^I} \approx \frac{b_0}{2D_c\mathcal{F}C_c^\infty}\exp\left\{\frac{-m_0\mathcal{F}\eta}{RT}\right\} \qquad [60]$$

Since $G_c/C_c^I > 0$, the interface is unstable for small ω and is stabilized by surface tension for sufficiently large ω. For the values listed in Table I, we have $m_0\Omega\gamma/RT = 2.80 \times 10^{-7}$ cm. For $\eta = -0.3$ V we then find that the system is stable for $\omega > 1.0 \times 10^4$ cm^{-1}. It is important to note that the kinetics used throughout this paper are for base electrolytes containing inhibiting polyethylene glycol (PEG) and chloride ions (Cl^{-1}), (concentrations given later) in addition to the catalyst; thus, in the limit of vanishing catalyst concentration, the kinetics modeled are those for the fully inhibited PEG-Cl-containing electrolyte.

Numerical Results

We have carried out numerical calculations for the parameter values given in Table I for various values of the bulk catalyst concentration C_a^∞ and the overpotential η. The numerical calculations were performed using the full dispersion relation given in Eq. 38, however, we also find that the approximate dispersion relation given by Eq. 40 is an excellent approximation, except at very small values of ω (*i.e.*, at longer wavelengths λ). We note that for very small values of ω we have found additional stable modes that play no role in the consideration of the stability of the system.

In Fig. 1 we show the real and imaginary parts of the temporal growth rate, σ_r and σ_i, as functions of the wavenumber ω for $\eta = -0.3$ V and $C_a^\infty = 1.0 \times 10^{-9}$ mol/cm^3. The associated steady-state surface coverage of catalyst and cupric ion concentration near the interface can be found in Table II. The system is stable ($\sigma_r < 0$) for wavenumbers greater than ω_c, where the critical wavenumber ω_c denotes the largest value of ω for which $\sigma_r = 0$. In Fig. 1, $\omega_c = 1289.9$ cm^{-1} ($\lambda_c = 49$ μm). The solid curves correspond to real modes ($\sigma_i = 0$), for which the temporal growth rate of the perturbation is monotonic (nonoscillatory) in time. The dashed curve in Fig. 1 corresponds to a complex mode with $\sigma_i \neq 0$, in which case the growth rate is oscillatory in time. For small ω, one of the real modes is stable and the other unstable. The unstable mode becomes stable at the critical wavenumber ω_c. At ω_c the values of $\hat{\theta}$ and $\hat{h}$ are 180° out of phase for both of the modes; that is, $\hat{\theta}/\hat{h}$ is real and negative. Thus the catalyst coverage and the deposition rate are enhanced in troughs and depressed on peaks, consistent with stabilization of the interface. At larger values of ω the two real modes merge into a complex mode with complex conjugate growth rates $\sigma_r \pm i\sigma_i$. The complex mode, with its negative σ_r, is stable for all wavenumbers. As ω increases further, σ_i steadily increases while σ_r decreases slightly; for example, for $\omega = 63052$ cm^{-1} ($\lambda = 1.004$ μm) we have $\sigma_r = -8.4 \times 10^{-4}$ s^{-1} and $\sigma_i = \pm 0.04$ s^{-1}.

In Fig. 2 we show σ_r and σ_i as functions of the wavenumber ω for $\eta = -0.3$ V and $C_a^\infty = 1.0 \times 10^{-13}$ mol/cm^3. There are again two real modes for small ω. However, both the real modes and the complex branch into which they merge are unstable ($\sigma_r \approx 5 \times 10^{-6}$ s^{-1}) for $\omega \approx 36$ cm^{-1}. For larger values of ω, σ_r increases to a maximum of about 10^{-5} s^{-1} for $\omega \approx 2000$ cm^{-1}, and then decreases steadily, with $\sigma_r = 0$ for $\omega_c = 13931.0$ cm^{-1} ($\lambda_c = 4.5$ μm), with stability for $\omega > \omega_c$ due to capillarity (not shown). For $\omega = 62355$ cm^{-1} ($\lambda = 0.99$ μm), the growth rate has further decreased to $\sigma_r = -1.82 \times 10^{-4}$ s^{-1}.

Tables II and III summarize the numerical results for different catalyst concentrations C_a^∞ at $\eta = -0.3$ V and $\eta = -0.2$ V, re-

Table III. Numerical results for $C_c^\infty = 2.78 \times 10^{-4}$ mol/cm^3 and $\eta = -0.2$ V.

C_a^∞ (mol/cm^3)	C_a^I (mol/cm^3)	10^5 C_c^I (mol/cm^3)	$\theta^{(0)}$	10^7 V (cm/s)	ω_c (cm^{-1})	σ_i (s^{-1})
1.0×10^{-7}	9.85×10^{-8}	6.87	0.260	5.34	1989.2	0
1.0×10^{-8}	9.83×10^{-9}	11.01	0.127	4.29	756.7	0
1.0×10^{-9}	9.82×10^{-10}	15.80	0.0605	3.06	304.2	0
1.0×10^{-10}	9.81×10^{-11}	19.97	0.0284	2.00	132.7	0
1.0×10^{-11}	9.81×10^{-12}	22.82	0.0133	1.27	63.31	0
1.0×10^{-12}	9.81×10^{-13}	24.45	0.00617	0.855	33.07	0
1.0×10^{-13}	9.80×10^{-14}	25.30	0.00287	0.640	18.82	0
1.0×10^{-14}	9.80×10^{-15}	25.71	0.00133	0.535	1384.0	3.19×10^{-5}

Table IV. Numerical results for $C_c^\infty = 2.78 \times 10^{-4}$ mol/cm^3 and $C_a^\infty = 1.0 \times 10^{-8}$ mol/cm^3.

η (V)	10^9 C_a^I (mol/cm^3)	C_c^I (mol/cm^3)	$\theta^{(0)}$	10^7 V (cm/s)	ω_c (cm^{-1})	σ_i (s^{-1})
−0.1	9.97	2.63×10^{-4}	0.0303	0.395	4.22×10^2	0
−0.2	9.83	1.10×10^{-4}	0.127	4.29	7.57×10^2	0
−0.3	9.08	1.18×10^{-5}	0.275	6.79	3.73×10^3	0
−0.4	6.31	1.20×10^{-6}	0.403	7.06	2.00×10^4	0
−0.5	2.19	1.45×10^{-7}	0.480	7.09	4.57×10^5	0.283

spectively. Table IV summarizes the results at different overpotentials η for $C_a^\infty = 1.0 \times 10^{-8}$ mol/cm^3. The values of the critical wavenumbers ω_c and the imaginary part of the growth rate σ_i at the onset of instability are given. Also included are the unperturbed values of the catalyst concentration at the interface C_a^I, the copper concentration at the interface C_c^I, the dimensionless coverage of adsorbed catalyst $\theta^{(0)}$, and the interface velocity V.

From Table II, C_a^I is approximately 90% of C_a^∞ over seven orders of magnitude of catalyst concentration. Thus, only a small concentration gradient of catalyst exists in the electrolyte for the kinetically limited catalyst accumulation. As C_a^∞ decreases, the steady-state coverage of adsorbed catalyst $\theta^{(0)}$ also decreases. With less adsorbed catalyst, the interface velocity (*i.e.*, the copper deposition rate) decreases, and the copper concentration at the interface increases towards the bulk value. For the smaller values of C_a^∞, the critical wavenumber corresponds to a complex mode, with a value of ω_c that tends toward a limiting value near 10^4 cm^{-1} as C_a^∞ decreases. For the larger values of C_a^∞, the critical wavenumber ω_c corresponds to a real mode with ω_c increasing as C_a^∞ increases.

The dependence of the critical wavenumber on the catalyst concentration summarized in Table II is also plotted in Fig. 3 (additional points have been added for clarity). The greatest stabilization of the surface is for the lowest value of ω_c, which occurs at about 300 cm^{-1} for catalyst concentration $C_a^\infty \approx 10^{-10}$ mol/cm^3 for $\eta = -0.3$ V. This optimum condition corresponds to the junction of the real and complex modes having $\sigma_r = 0$.

When the catalyst concentration falls to a value where the CEAC brightening mechanism no longer functions effectively, near $C_a^\infty = 10^{-11}$ mol/cm^3, destabilization is rapid. This sensitivity of ω_c to C_a^∞ for the complex modes arises from the near-independence of σ_r of these modes to wavenumber (see Fig. 1 and 2); because the σ_r curve for the complex mode is nearly horizontal, its intercept on the horizontal axis (*i.e.*, ω_c) is extremely sensitive to the vertical displacements of the curve associated with different values of C_a^∞. The more gradual increase of ω_c at the higher concentrations C_a^∞ associated with the real modes derives in part from the destabilizing cupric ion gradient associated with the increasing deposition rate.

Numerical results for $\eta = -0.2$ V are given in Table III, and the corresponding critical wavenumbers are also plotted in Fig. 3. The critical wavenumbers are lower than those for $\eta = -0.3$ V, indicating greater stability for any particular catalyst concentration C_a^∞. This is consistent with what would be expected for the smaller, destabilizing concentration gradient of the cupric ion, indicated by the reduced cupric ion depletion at the interface for deposition at −0.2 V (Tables II and III). The rapid increase of ω_c occurs at concentration C_a^∞ approximately two orders of magnitude lower than for depositions at $\eta = -0.3$ V and, again, marks a transition from real to complex modes. The increased stability is due, in some part, to the smaller cupric ion gradient at $\eta = -0.2$ V.

In terms of the stability criteria given in Eq. 50 and 51, the instability at $\omega < \omega_c$ for concentrations C_a^∞ with complex roots arises by violation of Eq. 50. For these lower concentrations C_a^∞ and associated coverages $\theta^{(0)}$, the right side of Eq. 50 is positive, and the mode is only stabilized by the surface tension term on the left side. For larger values of C_a^∞, the right side of Eq. 50 is negative, making the criterion satisfied for all wavenumbers, and Eq. 51 therefore determines stability.

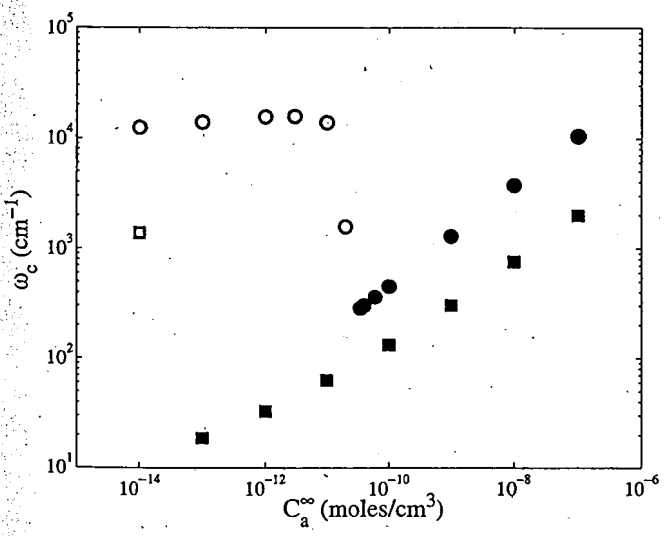

Figure 3. Critical wavenumber ω_c *vs.* C_a^∞ for $C_c^\infty = 2.78 \times 10^{-4}$ mol/cm^3. Closed symbols correspond to real modes, and open symbols correspond to complex modes (see Tables II and III). For $\eta = -0.3$ and −0.2 V, the data points are indicated by circles and squares, respectively. The system is stable for $\omega > \omega_c$.

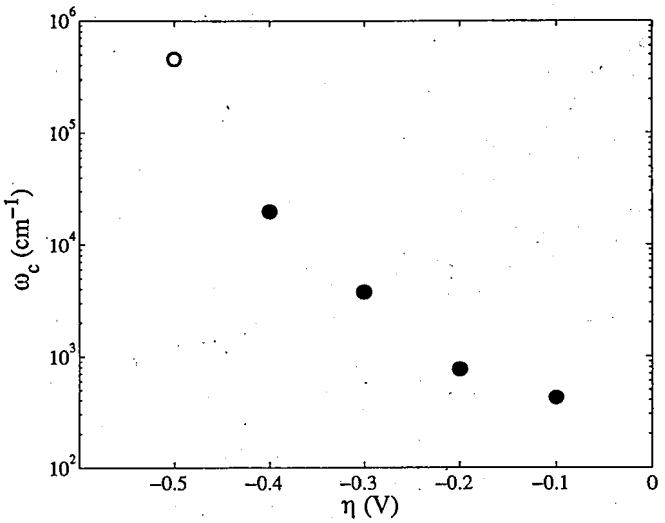

Figure 4. Critical wavenumber ω_c *vs.* η for $C_c^\infty = 2.78 \times 10^{-4}$ mol/cm^3 and $C_a^\infty = 1.0 \times 10^{-8}$ mol/cm^3. The open circle is a complex mode (see Table IV). The system is stable for $\omega > \omega_c$.

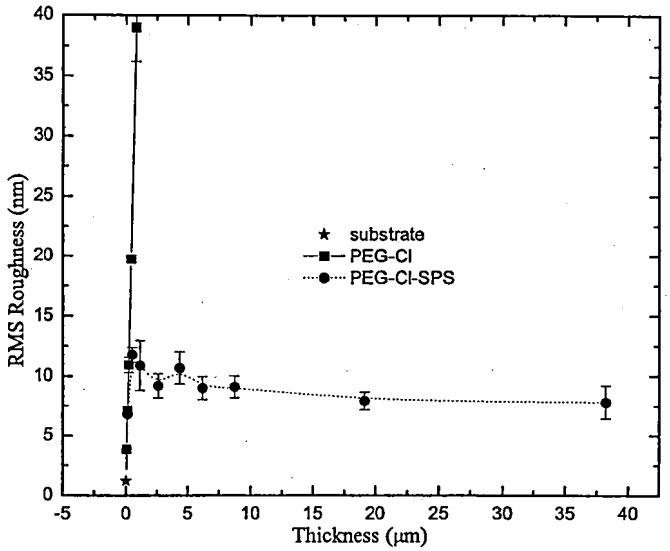

Figure 5. The measured rms roughness *vs.* deposit thickness with and without SPS in the electrolyte. Film thicknesses were determined by integrating the time-dependent deposition currents for each specimen using the known charge of the Cu^{2+} ions and the surface area of the deposits. Specimen thickness variation was obtained by changing deposition time alone.

Results for ω_c as a function of overpotential η for $C_a^\infty = 1.0 \times 10^{-8}$ mol/cm^3 are given in Table IV and Fig. 4. As η varies from -0.1 to -0.5 V, the system becomes increasing unstable; for $\eta = -0.5$ V the critical wavenumber corresponds to a complex mode.

Experimental Results

Comparison to experimental observations of the surface roughness of deposits provides strong support for the proposed mechanism. Roughness measurements were made for deposits from electrolytes with and without catalyst. Films were grown at a fixed overpotential of -0.25 V for fixed times, rinsed in distilled water, and transferred to an atomic force microscope (AFM) for roughness measurements. For the purposes of this work, only the saturation roughness for each specimen (the scan-length independent value obtained for sufficiently large scans) is presented.

Both electrolytes contained 0.25 mol/L $CuSO_4 \cdot 5H_2O$ and 1.8 mol/L H_2SO_4, 10^{-3} mol/L Cl^{-1}, and 88.2×10^{-6} mol/L of 3400 molecular weight polyethylene glycol (PEG) additives; the latter two components suppress copper deposition. A concentration of 6×10^{-6} mol/L of the disulfide catalyst $Na_2\ [SO_3(CH_2)_3S]_2$ was used for the catalyst containing electrolyte. The deposition rate and the kinetics for catalyst adsorption and consumption summarized in Table I and Eq. 5 and 6 as used in the modeling sections are representative of those obtained experimentally for this electrolyte-catalyst system.[25] Kinetics, aside from consumption, have also been published previously for a similar electrolyte-catalyst system.[18-21]

Figure 5 summarizes the thickness-dependent root-mean-square (rms) roughness of copper deposits made in the electrolytes. Because the modeling presented here is based on perturbations about steady-state deposition conditions, it is not expected to describe surface evolution during the approach to steady-state conditions, and thus the transient period of roughening in both electrolytes is not addressed here. More relevantly, after approximately 0.5 μm of deposition, the surface roughness of deposits from the electrolyte containing the SPS catalyst stabilizes and begins to attenuate slightly with further growth. This is consistent with the stabilization to very long wavelengths (very small ω_c) predicted by the model for this overpotential and catalyst concentration (Fig. 3). In contrast, the deposits from the electrolyte with no catalyst continue to roughen, with rms roughness reaching 70 nm rms at 300 s.

It is worth noting that, at -0.25 V overpotential, the steady-state metal deposition rate in the catalyst-containing electrolyte is approximately four times faster than that in the catalyst-free electrolyte. The corresponding depletion of cupric ion at the growth surface is approximately 20% from the bulk concentration for the catalyst-free electrolyte *vs.* approximately 85% for the catalyst-containing electrolyte; these values are based on steady-state currents for deposition under the given conditions (not shown). Thus, the deposits from the catalyst-containing electrolyte are smoother in spite of having been grown in a steeper metal-ion concentration gradient in the electrolyte. A more thorough comparison of modeling and experimental results will be published separately.

Discussion

The long-term saturation, and attenuation, of roughness observed experimentally is as predicted. These results suggest that the CEAC mechanism originally proposed to describe superconformal filling of vias and trenches can also function as a mechanism for creating bright, planar deposits.

These results clearly indicate a potential mechanism by which catalyst containing electrolytes can maintain planar surfaces during deposition, yielding bright deposits (subject to instabilities at larger length scales that arise from the finite boundary layer thickness). Interestingly, there is predicted to be no stabilization absent competition between accumulation and consumption establishing the coverage. Thus no stabilization is predicted for a system where an initial coverage of catalyst is achieved prior to deposition with negligible accumulation or consumption during the metal deposition process. Therefore, this result, while explaining how catalyst-containing electrolytes yield bright deposits, does not explain why reduced roughness is also observed in experiments where catalyst is adsorbed on surfaces prior to metal deposition. Such an explanation might be obtained by going to higher order in the stability analysis to seek a stable state with a finite, nonzero perturbation amplitude.

It is presumptuous to extract much more than the largest length scale for which a perturbation is stable from a first-order perturbation analysis. Nonetheless, it is worth noting that complex exponents, with a negative real component, mean that some perturbations will decay in an oscillatory manner. In such a case the deposit thickness at a particular location will exhibit oscillatory deviations from the average growth surface, with successively smaller maximum positive and negative deviations with time. It was noted at the start of this work that the CEAC mechanism responsible for the brightening presented here also causes the bottom-to-top filling of submicrometer features. Such filling is typically followed by development of an overfill bump that subsequently decays back to the planar growth front.[18-20,23] This behavior is analogous to the damped oscillatory behavior described above.

Acknowledgments

The authors are grateful for helpful discussions with K. F. Gurski and J. E. Guyer. We acknowledge partial support of this work from the NASA Physical Sciences Division.

National Institute of Standards and Technology assisted in meeting the publication costs of this article.

References

1. W. W. Mullins and R. F. Sekerka, *J. Appl. Phys.*, **35**, 444 (1964).
2. S. R. Coriell and G. B. McFadden, in *Handbook of Crystal Growth*, Vol. 1B, p. 785, D. T. J. Hurle, Editor, Elsevier, Amsterdam (1993).
3. R. Aogaki, K. Kitazawa, Y. Kose, and K. Fueki, *Electrochim. Acta*, **25**, 965 (1980).
4. R. Aogaki and T. Makino, *Electrochim. Acta*, **26**, 1509 (1981).
5. R. Aogaki, *J. Electrochem. Soc.*, **129**, 2442 (1982).
6. R. Aogaki and T. Makino, *J. Electrochem. Soc.*, **131**, 40 (1984).
7. R. Aogaki and T. Makino, *J. Chem. Phys.*, **81**, 2154 (1984).
8. R. Aogaki and T. Makino, *J. Chem. Phys.*, **81**, 2164 (1984).
9. D. P. Barkey, R. H. Muller, and C. W. Tobias, *J. Electrochem. Soc.*, **136**, 2199 (1989).

10. D. P. Barkey, R. H. Muller, and C. W. Tobias, *J. Electrochem. Soc.*, **136**, 2207 (1989).
11. C.-P. Chen and J. Jorne, *J. Electrochem. Soc.*, **138**, 3305 (1991).
12. C. H. J. Van Den Brekel and A. K. Jensen, *J. Cryst. Growth*, **43**, 364 (1978).
13. C. H. J. Van Den Brekel and A. K. Jensen, *J. Cryst. Growth*, **43**, 371 (1978).
14. C. Madore, M. Matlosz, and D. Landolt, *J. Electrochem. Soc.*, **143**, 3927 (1996), and numerous references therein.
15. C. Madore and D. Landolt, *J. Electrochem. Soc.*, **143**, 3936 (1996).
16. D. Roha and U. Landau, *J. Electrochem. Soc.*, **137**, 824 (1990).
17. A. C. West, *J. Electrochem. Soc.*, **147**, 227 (2000).
18. T. P. Moffat, D. Wheeler, W. H. Huber, and D. Josell, *Electrochem. Solid-State Lett.*, **4**, C26 (2001).
19. D. Josell, D. Wheeler, W. H. Huber, and T. P. Moffat, *Phys. Rev. Lett.*, **87**, article no. 016102 (2001).
20. D. Wheeler, D. Josell, and T. P. Moffat, *J. Electrochem. Soc.*, **150**, C302 (2003).
21. D. Josell, D. Wheeler, W. H. Huber, J. E. Bonevich, and T. P. Moffat, *J. Electrochem. Soc.*, **148**, C767 (2001).
22. D. Josell, D. Wheeler, and T. P. Moffat, *Electrochem. Solid-State Lett.*, **5**, C49 (2002).
23. D. Josell, D. Wheeler, and T. P. Moffat, *Electrochem. Solid-State Lett.*, **5**, C44 (2002).
24. F. R. Gantmacher, *The Theory of Matrices*, Vol. II, Chelsea, New York (1959).
25. T. P. Moffat, Unpublished results.

Solution 11 - Control w/ Acetate Salts

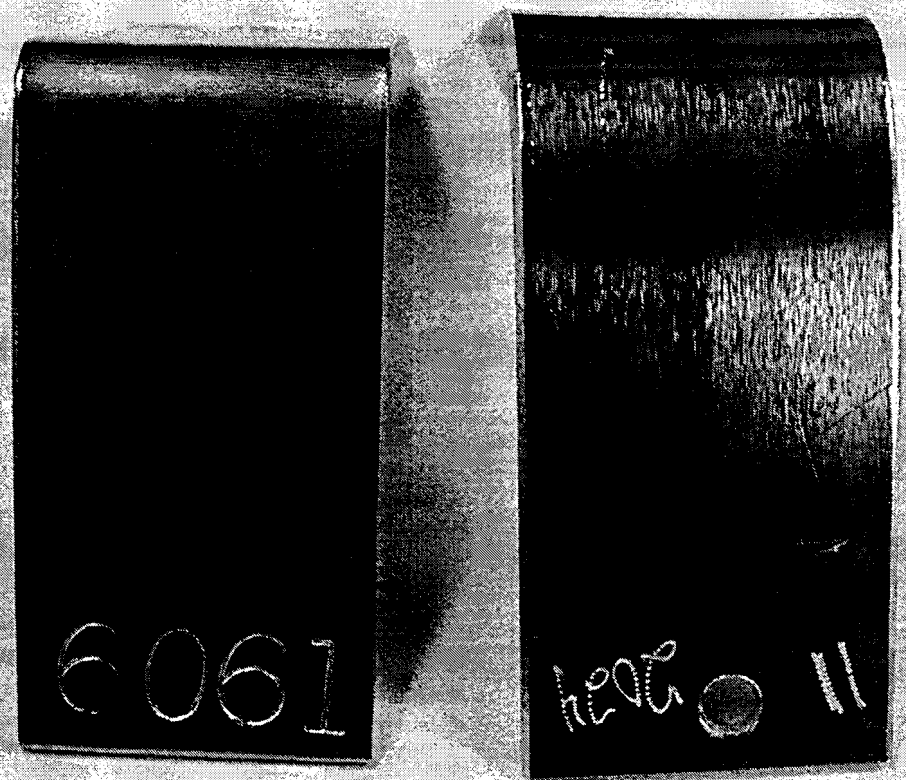

6061 2024

EXHIBIT
B

Solution 12 - Chloride Salts

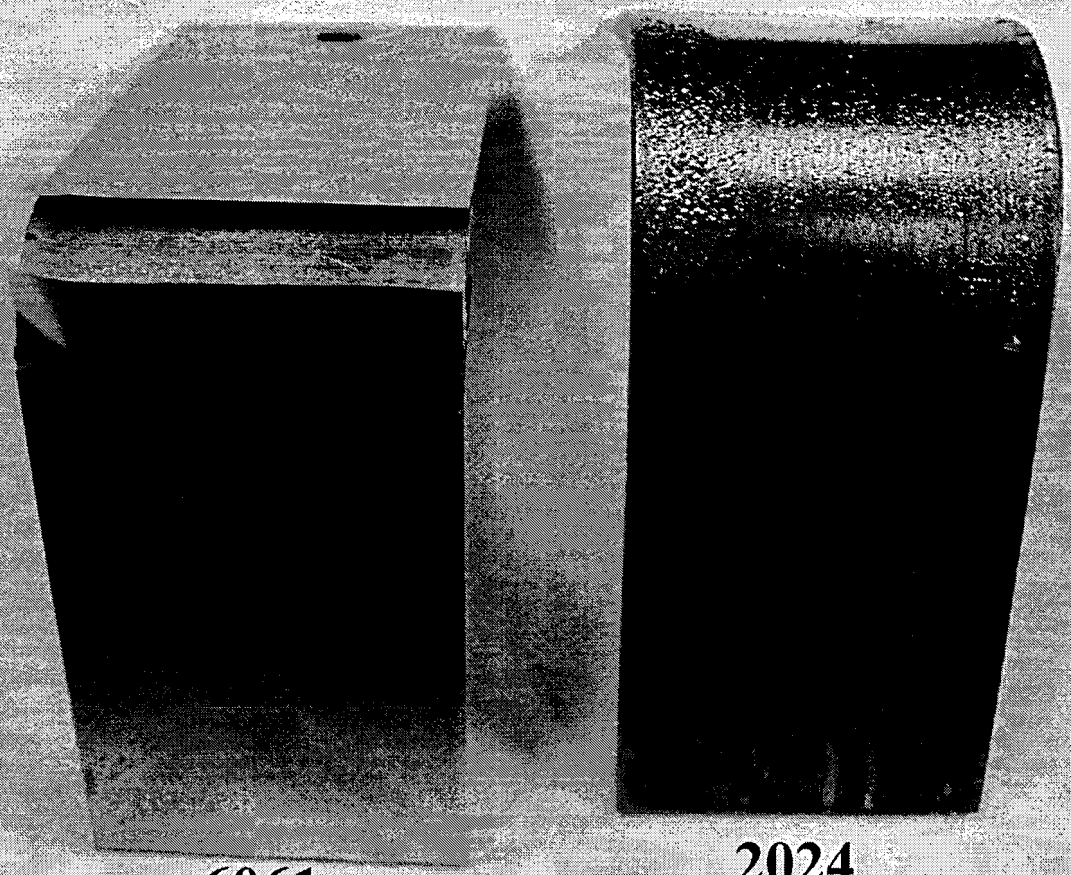

6061

2024

EXHIBIT
C

Solution 13 - Sulfate Salts

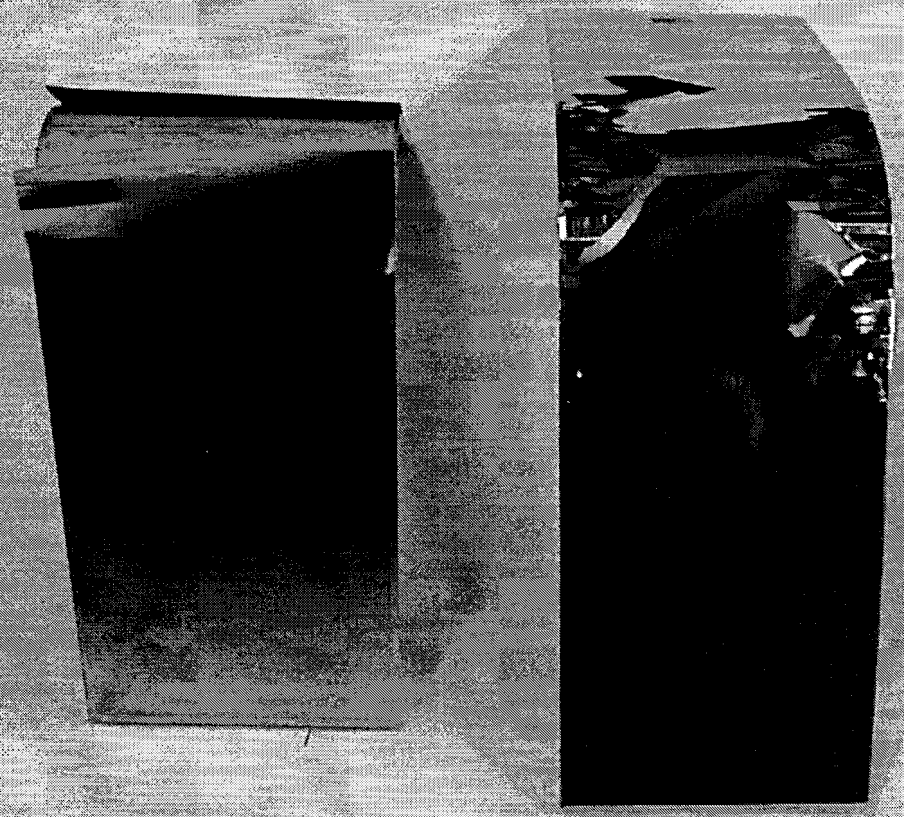

6061 2024

EXHIBIT
D

INZ Solution w/ Acetate Salts - pH 4.0

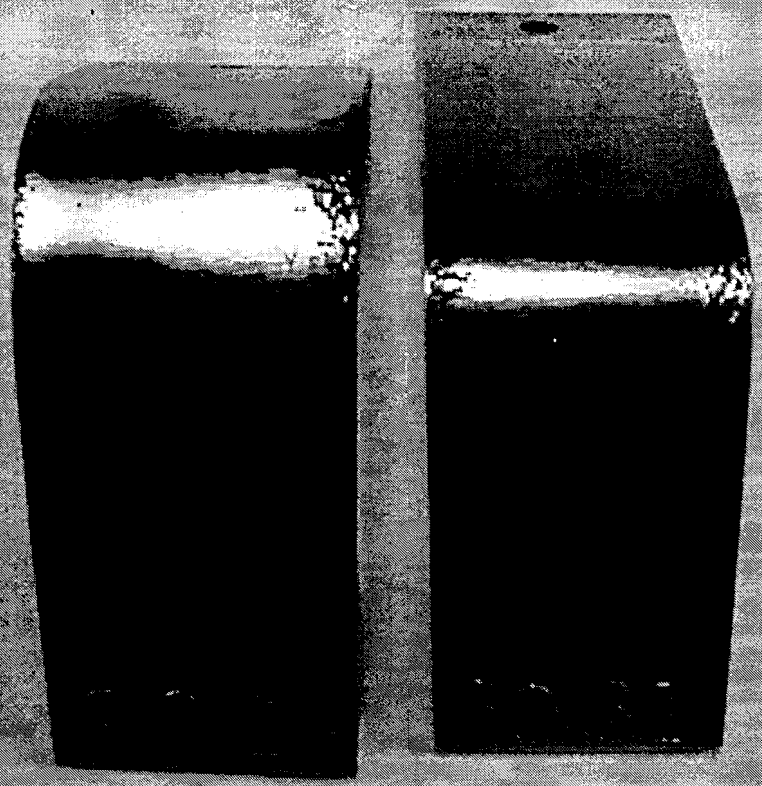

2024 6061

EXHIBIT
E

INZ Solution w/ Acetate Salts - pH 5.0

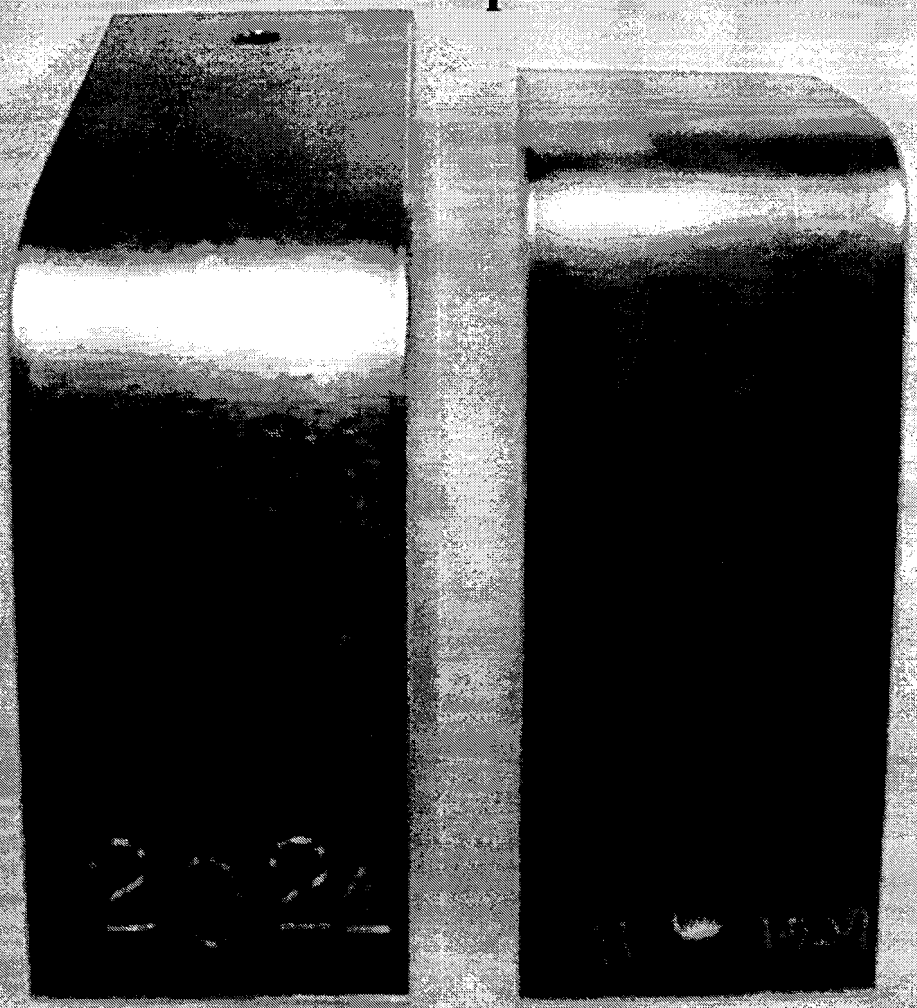

2024 6061

EXHIBIT F

INZ Solution w/ Acetate Salts - pH 6.0

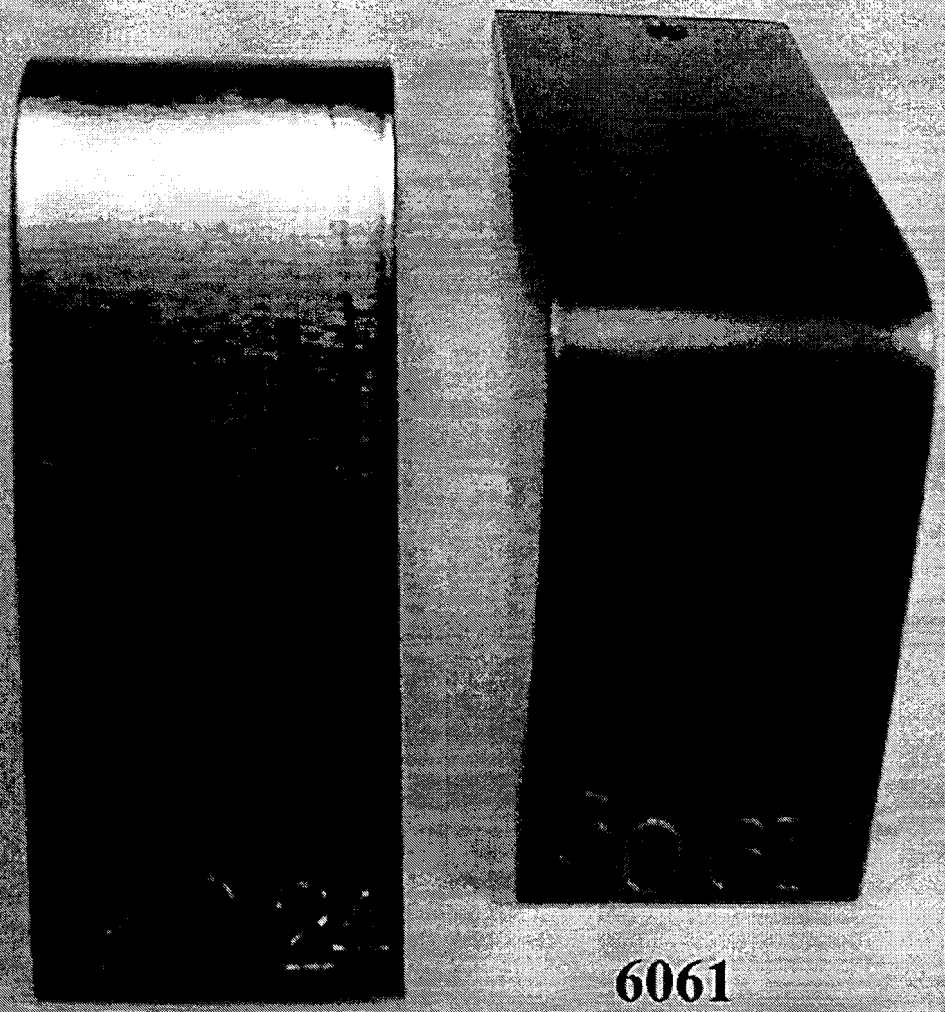

2024

6061

EXHIBIT
G